JPEDAV (2015) 36:493–502
DOI: 10.1007/s11669-015-0405-3
1547-7037 ©ASM International

# Phase Equilibria of the Cu-Si-Sn System at 700 and 500 °C

*Yuanyuan Song, Xuping Su, Ya Liu, Haoping Peng, Changjun Wu, and Jianhua Wang*

*(Submitted April 22, 2015; in revised form August 17, 2015; published online September 9, 2015)*

**Intermetallic compounds formed in solder joints have a substantial effect on reliability. Because Sn-based alloys are alternatives to lead-containing solders, phase equilibria of the Cu-Si-Sn system were investigated for quenched samples annealed at 700 and 500 °C for 30 days. Nine three-phase equilibria were well established at 700 °C, and a previously unknown ternary τ phase with a possible homogeneity interval in the range $Cu_{76}Sn_{7.8}Si_{16.2}$-$Cu_{85}Sn_{7.6}Si_{7.4}$ was found for the first time. The τ phase has a hexagonal structure with $a$ = 8.012 nm and $c$ = 5.04 nm. Six three-phase regions were identified in the isothermal region at 500 °C. In contrast with the isothermal region at 700 °C, the new ternary τ phase was not observed at 500 °C. The solubility of Si in ε-$Cu_3Sn$ decreases from 12.8 to 1.4 at.%, and only small variations occur in the homogeneity ranges of η-$Cu_3Si$ and γ-$Cu_5Si$.**

**Keywords** Cu-Si-Sn system, intermetallics, phase equilibria
Sn-based solder

## 1. Introduction

Lead-containing solders, mainly Sn63-Pb37 eutectic alloy, have been widely used in electronics packaging for more than 50 years. However, because lead is a toxic metal and is harmful to health, the requirement to ban the use of lead in the electronics industry, at least in consumer electronics, is increasing throughout the world. Therefore, development of environment-friendly solder, i.e. Pb-free solder, has been of great concern in recent years.[1-4]

Sn-based alloys are well known Pb-free solders. A Cu-Sn intermetallic compound (IMC) forms at the solder-copper interface.[5-8] Recently, it has been reported that growth of the Cu-Sn IMC layer has a crucial effect on solder joint reliability. With increasing thickness of the $Cu_6Sn_5$ IMC layer, the thermal fatigue life,[9,10] isothermal shear fatigue life,[11] tensile strength,[12] and fracture toughness[13] of solder joints decrease. Therefore, restricting the growth of the Cu-Sn IMC should be an effective means of improving the reliability of solder joints. To develop Sn-based solder, it is important to identify the intermetallic compounds formed in microelectronic joints and study their mechanical properties.[14] Because it is well known that addition of silicon to silicon monel alloys has improved this alloy's strength, ductility, corrosion resistance, and wear resistance,[15] we investigated addition of silicon to the Cu-Sn system to improve the mechanical properties of the solder. Little attention has been devoted to the Cu-Si-Sn ternary system, no information is available about it, so research on the phase equilibria of this system is necessary.

There are three boundary binary systems, Cu-Si, Cu-Sn and Si-Sn, in the Cu-Si-Sn ternary system. According to Okamoto[16] ten solid phases (fcc-Cu, diamond-Si, β-bcc and κ-$Cu_{6.69}Si$, δ-$Cu_{33}Si_7$, γ-$Cu_5Si$, ε-$Cu_{15}Si_4$, η-$Cu_3Si$, η′-$Cu_3Si$, and η″-$Cu_3Si$) are present in the Cu-Si system. Except for diamond-Si all of these phases have solubility ranges. In the latest thermodynamic assessment by Shin et al. [17] the ordered intermetallic phases (δ-$Cu_{33}Si_7$, γ-$Cu_5Si$, ε-$Cu_{15}Si_4$, η-$Cu_3Si$, η′-$Cu_3Si$, and η″-$Cu_3Si$) were regarded as stoichiometric and the polymorphs of the η-$Cu_3Si$ phase were ignored, i.e. the review by Okamoto was accepted. The Cu-Sn system has been optimized by Shim et al.,[18] Miettinen,[19] Liu et al.,[20] Gierlotka et al.,[21] and Li et al.[22] by use of Calphad software. More recently, Fürtauer et al.[23] investigated the Cu-Sn system, devoting special attention to the high-temperature phases β(W-type) and γ($BiF_3$-type), and a higher-order transformation between these two phases was described. The new findings were included in a new thermodynamic assessment of this Cu-Sn system, in which ten phases are included, namely, liquid, fcc-Cu, β-bcc (A2), γ-bcc (D0_3), δ-$Cu_{41}Sn_{11}$, ζ-$Cu_{10}Sn_3$, ε-$Cu_3Sn$, η-$Cu_6Sn_5$, η′-$Cu_6Sn_5$, and Sn.[24] To facilitate reading, the experimentally determined Cu-Sn phase diagram is shown in Fig. 1. The data for the Si-Sn system are from Ref 25, in which no IMC was reported. The main crystallographic data and phase stability of the boundary of the unary and binary phases of the Cu-Si-Sn system are summarized in Table 1.

**Yuanyuan Song, Xuping Su, Haoping Peng, Changjun Wu,** and **Jianhua Wang**, School of Materials Science and Engineering, Changzhou University, Changzhou 213164, China and Jiangsu Key Laboratory of Materials Surface Science and Technology, Changzhou University, Changzhou 213164, China; and **Ya Liu**, School of Materials Science and Engineering, Changzhou University, Changzhou 213164, China; Jiangsu Key Laboratory of Materials Surface Science and Technology, Changzhou University, Changzhou 213164, China; and Jiangsu Collaborative Innovation Center of Photovolatic Science and Engineering, Changzhou University, 13164 Jiangsu, People's Republic of China. Contact e-mails: clsj@cczu.edu.cn and sxping@cczu.edu.cn.

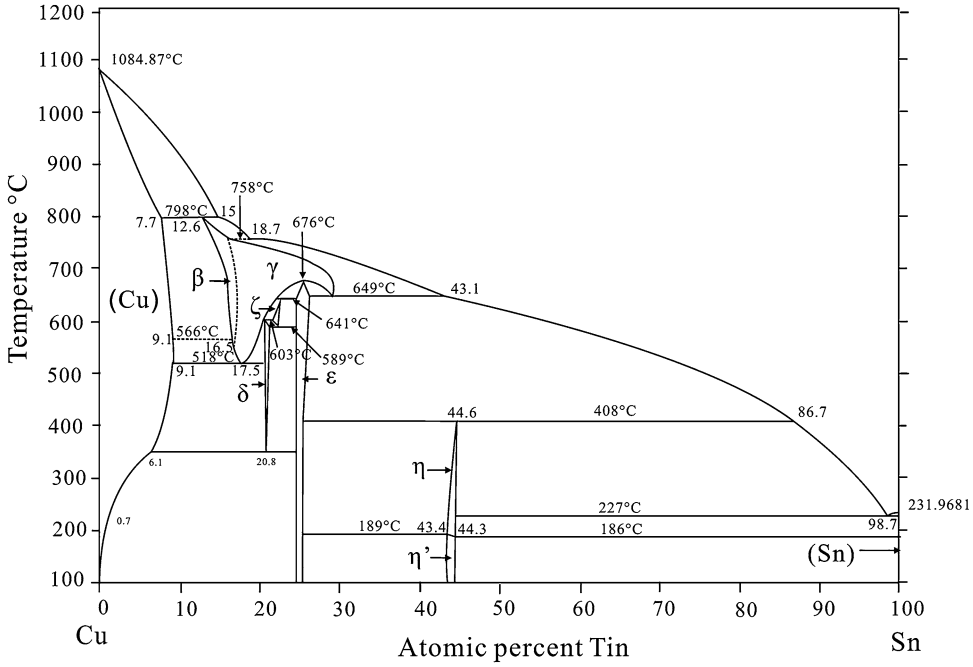


**Fig. 1** Phase diagram of the Cu-Sn binary system[21]

**Table 1 Crystallographic data for the binary compounds in the Cu-Si-Sn system**

| Phase | Crystal system | Space group | Lattice constants (nm) | | | Domain of stability (°C) | Composition range (700 °C) | Composition range (500 °C) | Refs. |
|---|---|---|---|---|---|---|---|---|---|
| | | | *a* | *b* | *c* | | | | |
| (Cu) | Cubic | *Fm*-3 *m* | 3.615 | 3.615 | 3.615 | <1084.87 | <9 at.% Sn, <11.5 at.% Si | <10 at.% Sn, <10.5 at.% Si | [24,27] [26] |
| Liq. | Tetragonal | $I4_1/amd$ | 5.831 | - | 3.182 | <231.9 | <65 at.% Cu, <1 at.% Si | <23 at.% Cu, <1 at.% Si | [23,24] [25,28] |
| (Si) | Diamond | *Fd*-3*m* | 4.737 | 4.502 | 2.55 | <1414.4 | <1 at.% Cu, <1 at.% Sn | <1 at.% Cu, <1 at.% Sn | [26] [25] |
| $\kappa$-$Cu_{6.69}Si$ | Hexagonal | *P*63/*mmc* | 2.561 | - | 4.184 | 552-842 | 85.5-89 at.% Cu | - | [17,35] |
| $\delta$-$Cu_{33}Si_7$ | Hexagonal | *P*63/*mmc* | | | | 710-824 | - | - | [17] |
| $\beta$-$Cu_{0.87}Si_{0.13}$ | Cubic | *Im*-3*m* | | | | 785-852 | - | - | [17] |
| $\gamma$-$Cu_5Si$ | Cubic | $P4_132$ | 6.22 | 6.22 | 6.22 | <400-729 | 82.4-82.9 at.% Cu | 81.5-83 at.% Cu | [17,36] |
| $\varepsilon$-$Cu_{15}Si_4$ | Cubic | *I*-43*d* | 9.694 | 9.694 | 9.694 | <400-800 | 78.7-78.8 at.% Cu | 78.7-78.8 at.% Cu | [17,37] |
| $\eta$-$Cu_3Si$ | Orthorhombic | *P* | 6.041 | 6.356 | 4.288 | 558-859 | 75.1-77.8 at.% Cu | - | [17,38] |
| $\eta'$-$Cu_3Si$ | Orthorhombic | *P* | | | | 467-620 | - | 74.8-76.8 at.% Cu | [25] |
| $\eta''$-$Cu_3Si$ | Orthorhombic | *P* | | | | <400-570 | - | 75.1-76.5 at.% Cu | [17] |
| $\beta$-bcc (A2) | Cubic | *Im*-3*m* | 3.026 | 3.026 | 3.026 | 586-789 | 14-15 at.% Sn | - | [29] |
| $\gamma$-bcc (D0_3) | Cubic | *Fm*-3*m* | 6.117 | 6.117 | 6.117 | 520-755 | 16-25 at.% Sn | - | [29] |
| $\delta$-$Cu_{41}Sn_{11}$ | Cubic | *F*-43*m* | 17.980 | 17.980 | 17.980 | 350-640 | - | 20-20.5 at.% Sn | [30] |
| $\zeta$-$Cu_{10}Sn_3$ | Hexagonal | $P6_3/m$ | 7.330 | - | 7.870 | 582-590 | - | - | [31] |
| $\varepsilon$-$Cu_3Sn$ | Orthorhombic | *Cmcm* | 5.529 | 47.75 | 4.323 | <100-678 | - | 24.7-25.2 at.% Sn | [32] |
| $\eta$-$Cu_6Sn_5$ | Hexagonal | $P6_3/mmc$ | 4.192 | - | 5.037 | 186 ~ 415 | - | - | [33] |
| $\eta'$-$Cu_6Sn_5$ | Monoclinic | *C*2/*c* | 11.022 | 7.282 | 9.827 | <100-189 | - | - | [34] |

**Table 2 Summary of all the samples' nominal compositions, and experimental results for the Cu-Si-Sn alloys annealed at 700°C**

| | Nominal composition | | | | Phase composition | | |
|---|---|---|---|---|---|---|---|
| No. | Cu | Sn | Si | Phase | Cu | Sn | Si |
| #1 | 70 | 20 | 10 | η-$Cu_3Si$ | 76.3 | 5.6 | 18.1 |
| | | | | γ-bcc (D0_3) | 76.3 | 21.9 | 1.8 |
| | | | | Liq. | 56.8 | 43.0 | 0.2 |
| #2 | 30 | 20 | 50 | η-$Cu_3Si$ | 75.0 | 0.5 | 24.5 |
| | | | | Liq. | 53.0 | 45.5 | 1.5 |
| | | | | (Si) | 0.2 | 0.0 | 99.8 |
| #3 | 75 | 18 | 7 | η-$Cu_3Si$ | 75.0 | 0.5 | 24.5 |
| | | | | γ-bcc (D0_3) | 75.3 | 17.4 | 7.3 |
| | | | | Liq. | 40.3 | 59.1 | 0.6 |
| #4 | 64 | 19 | 17 | Liq. | 60.3 | 37.5 | 2.2 |
| | | | | η-$Cu_3Si$ | 75.7 | 0.6 | 23.7 |
| #5 | 70 | 20 | 10 | η-$Cu_3Si$ | 76.6 | 4.6 | 18.8 |
| | | | | γ-bcc (D0_3) | 75.1 | 23.2 | 1.7 |
| | | | | Liq. | 10.8 | 88.6 | 0.6 |
| #6 | 73 | 12 | 15 | γ-bcc (D0_3) | 75.6 | 22.9 | 1.5 |
| | | | | η-$Cu_3Si$ | 74.3 | 19.9 | 5.8 |
| | | | | Liq. | 60.3 | 37.1 | 2.6 |
| #7 | 76 | 8 | 16 | η-$Cu_3Si$ | 77.1 | 2.1 | 20.8 |
| | | | | γ-bcc (D0_3) | 74.9 | 18.8 | 6.3 |
| | | | | τ | 76.0 | 7.8 | 16.2 |
| #8 | 77 | 3 | 20 | τ | 77.9 | 9.3 | 12.8 |
| | | | | η-$Cu_3Si$ | 76.4 | 2.0 | 21.6 |
| #9 | 76 | 14 | 10 | τ | 76.3 | 7.3 | 16.4 |
| | | | | γ-bcc (D0_3) | 76.4 | 12.0 | 11.6 |
| #10 | 78 | 14 | 8 | γ-bcc (D0_3) | 79.2 | 13.4 | 7.4 |
| #11 | 79 | 10 | 11 | γ-$Cu_5Si$ | 79.6 | 5.8 | 14.6 |
| | | | | γ-bcc (D0_3) | 79.0 | 11.9 | 9.1 |
| | | | | τ | 76.8 | 9.3 | 13.9 |
| #12 | 80 | 10 | 10 | γ-bcc (D0_3) | 78.7 | 10.5 | 10.8 |
| | | | | γ-$Cu_5Si$ | 80.7 | 3.7 | 15.6 |
| #13 | 87 | 8 | 5 | (Cu) | 91.3 | 3.3 | 5.4 |
| | | | | γ-bcc (D0_3) | 85.3 | 10.3 | 4.4 |
| #14 | 81 | 2 | 17 | γ-$Cu_5Si$ | 80.7 | 3.8 | 15.5 |
| | | | | ε-$Cu_{15}Si_4$ | 79 | 0.5 | 20.5 |
| | | | | τ | 77.6 | 5.4 | 17.0 |
| #15 | 85 | 2 | 13 | κ-$Cu_{6.69}Si$ | 85.9 | 1.0 | 13.1 |
| | | | | γ-$Cu_5Si$ | 82.9 | 4.1 | 13 |
| #16 | 89 | 9 | 2 | (Cu) | 91.1 | 8.8 | 0.1 |
| | | | | β-bcc (A2) | 85.2 | 14.4 | 0.4 |
| #17 | 80 | 14 | 6 | γ-bcc (D0_3) | 79.9 | 13.9 | 6.2 |
| #18 | 82 | 13 | 5 | γ-bcc (D0_3) | 81.0 | 15.5 | 3.5 |
| #19 | 83 | 14 | 3 | β-bcc (A2) | 85.1 | 12.7 | 2.2 |
| | | | | γ-bcc (D0_3) | 80.1 | 16.3 | 3.6 |
| #20 | 84 | 15 | 1 | γ-bcc (D0_3) | 81.4 | 15.2 | 3.4 |
| | | | | β-bcc (A2) | 84.5 | 11.5 | 4.0 |
| #21 | 85 | 14 | 1 | β-bcc (A2) | 84.9 | 14.0 | 1.1 |
| #22 | 80 | 11 | 9 | γ-bcc (D0_3) | 81.5 | 12.1 | 6.4 |
| | | | | τ | 85.0 | 7.6 | 7.4 |
| #23 | 86 | 7 | 7 | γ-bcc (D0_3) | 81.4 | 12.8 | 5.8 |
| | | | | κ-$Cu_{6.69}Si$ | 85.3 | 5.9 | 8.8 |
| | | | | (Cu) | 90.5 | 2.2 | 7.3 |
| #24 | 87 | 8 | 5 | γ-bcc (D0_3) | 82.3 | 14.9 | 2.8 |
| | | | | (Cu) | 84.1 | 14.0 | 1.9 |
| #25 | 87 | 3 | 10 | (Cu) | 89.7 | 2.3 | 8 |
| | | | | κ-$Cu_{6.69}Si$ | 85.4 | 8.3 | 6.3 |
| #26 | 87 | 4 | 9 | γ-bcc (D0_3) | 86.0 | 1.2 | 12.8 |
| | | | | κ-$Cu_{6.69}Si$ | 82.0 | 11.0 | 7.0 |
| | | | | (Cu) | 85.2 | 5.9 | 8.9 |
| #27 | 81 | 8 | 11 | γ-$Cu_5Si$ | 80.8 | 5.5 | 13.7 |
| | | | | γ-bcc (D0_3) | 81.1 | 12.3 | 6.6 |

The alloy compositions are all in at.% in this paper. Compositions of the γ-bcc (D0_3) phase were determined by using the quenched phases at room temperature

Because:

1. no investigation has been devoted to the relationships between the phases in the Cu-Si-Sn system;
2. systematic research over the whole concentration range is helpful for finding new ternary phases; and
3. phase relationships can supply useful information about the stability of the compounds formed in the Sn-based alloy.

In this study we mainly determined the isothermal sections of the Cu-Si-Sn system for two temperatures, 700 and 500 °C. Because most of the binary compounds occur between 500 and 700 °C, phase relationships at these two temperatures are critical to understanding the phase relationships in the vertical section. This work would be helpful for identifying IMC formed in Cu-Si-Sn alloys and supply useful information for the development of Sn-based solders.

## 2. Experimental

In this study, copper sheets (99.99 wt.%), tin blocks (99.99 wt.%) and silicon particles (99.99 wt.%) were used as raw material to prepare ternary alloys. The nominal composition of the samples is listed in Table 2. The mass of each sample was approximately 5-6 g. Calculated amounts of the three materials were weighed with an accuracy of 0.01 mg. Under high-purity Ar gas the weighed samples were heated to the estimated liquidus temperature by arc

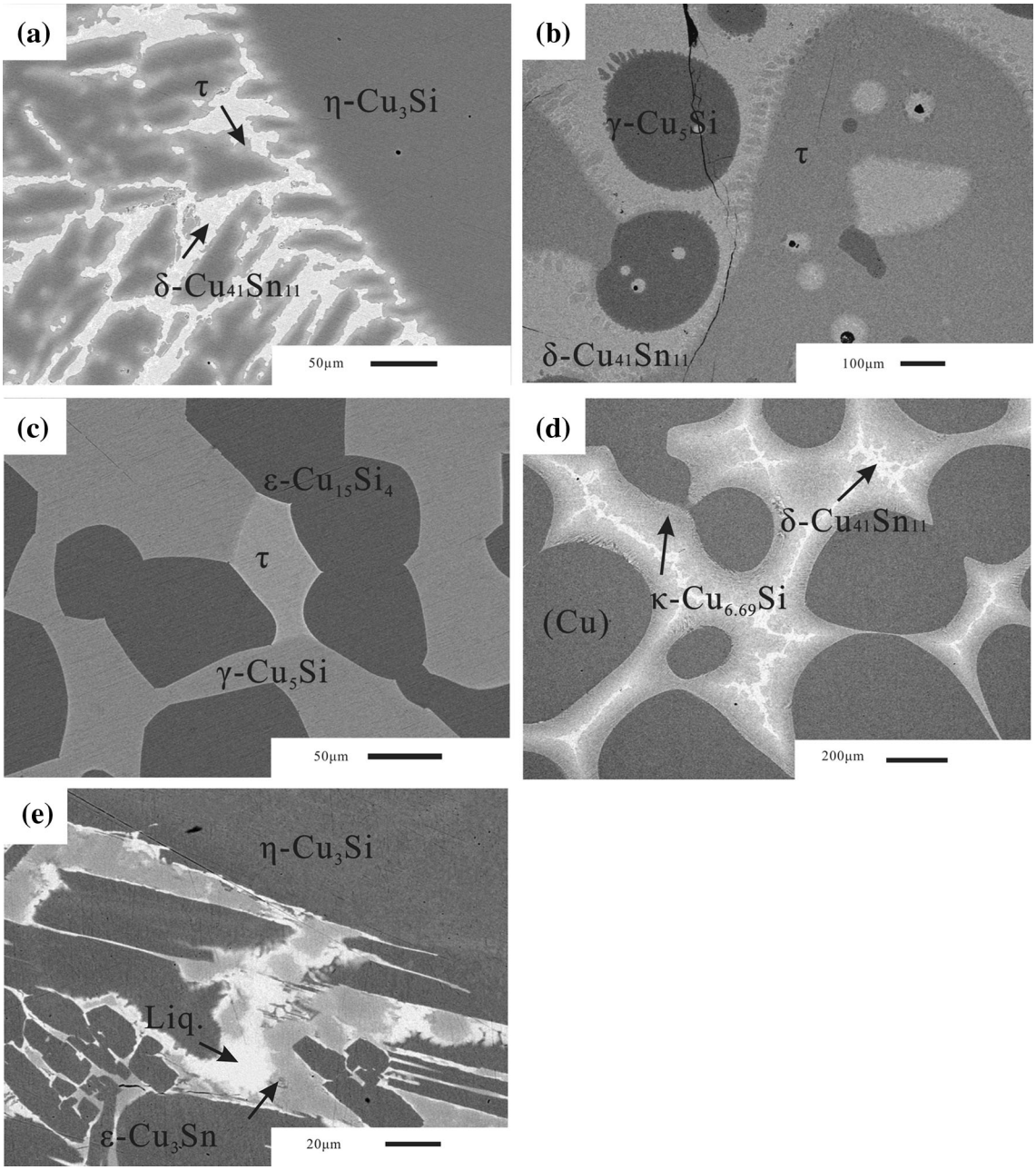


**Fig. 2** Images of the microstructure of typical ternary Cu-Si-Sn alloys annealed at 700 °C for 30 days. (a) #7 sample ($Cu_{76}Sn_8Si_{16}$), (b) #11 sample ($Cu_{79}Sn_{10}Si_{11}$), (c) #14 sample ($Cu_{81}Sn_2Si_{17}$), (d) #23 sample ($Cu_{86}Sn_7Si_7$), (e) #6 sample($Cu_{73}Sn_{12}Si_{15}$)

melting. The samples were overturned three times to achieve homogeneity. The samples were then re-sealed in evacuated quartz tubes and annealed at 500 or 700 °C for 30 days. Finally, all were quenched in cold water.

All of these equilibrated samples were cut into two parts. One part was used to identify the structures of phases by use of x-ray diffraction (XRD) analysis. XRD patterns were generated by use of a D/max 2500 PC x-ray diffractometer with Cu K$\alpha$ radiation and steps of 0.02° in the 2$\theta$ angle. Si powder was used as external calibrated standard. The Jade software package was used to index and calculate the XRD patterns. Samples studied by use of XRD were ground powders. The other part was used for micro-structural and analysis of phase composition by scanning electron microscopy (SEM), by use of a JSM-6510, and energy-dispersive x-ray spectroscopy (EDS) with an Oxford INCA with probe diameter of 1 μm and an accelerating voltage of 20 kV.

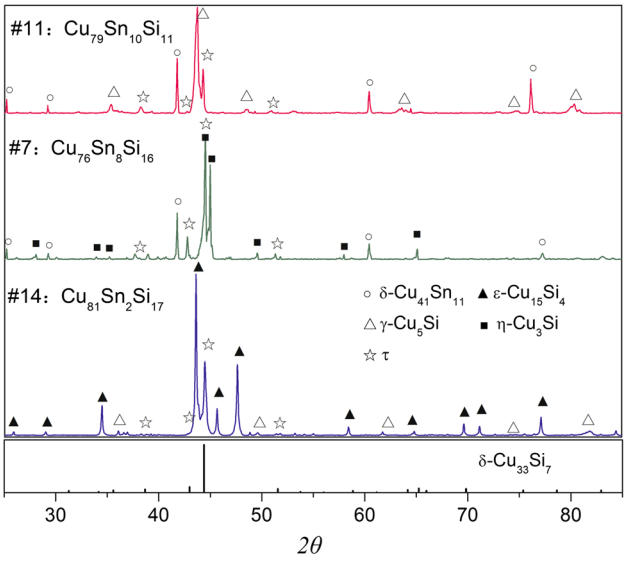


**Fig. 3** XRD patterns of typical alloys consisting of the new τ phase

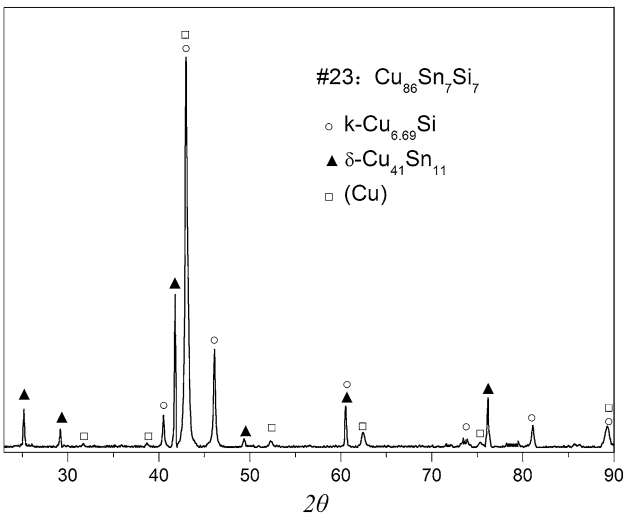


**Fig. 4** XRD pattern of alloy #23 ($Cu_{86}Sn_7Si_7$)

## 3. Results and Discussion

### 3.1 Phase Equilibria of the Cu-Si-Sn System at 700 °C

Figures 2a-e show images of the microstructure of typical ternary Cu-Si-Sn alloys annealed at 700°C for 30 days. XRD patterns of these representative ternary alloys are presented in Fig. 3-5. The nominal compositions of the alloys and the phases in the phase equilibria identified by a combination of XRD and SEM-EDS are listed in Table 2.

On the basis of backscattered electron images (BEI) and XRD patterns of the samples, shown in Fig. 2 and 3, respectively, four binary phases, η-$Cu_3Si$, ε-$Cu_{15}Si_4$, γ-$Cu_5Si$, and κ-$Cu_{6.69}Si$ were confirmed in the Cu-Si system. The solubility of Sn in these four Cu-Si phases was 5.6, 0.5, 5.8, and 1.2 at.%, respectively. No compound was present in the Sn-Si phase diagram, in accordance with Ref 25. However, the Cu-Sn system was much more complicated. According to the Cu-Sn phase diagram shown in Fig. 1, binary compounds γ-bcc (D0_3) and β-bcc (A2) should be stable at 700 °C. However, the binary phases determined from the quenched samples were δ-$Cu_{41}Sn_{11}$, ε-$Cu_3Sn$, or even η-$Cu_6Sn_5$. The detailed reasons will be explained during the interpretation of the experimental results, below.

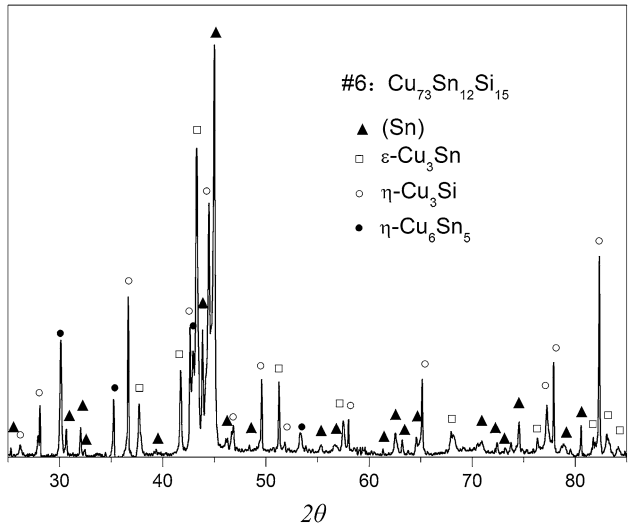


**Fig. 5** XRD pattern of #6 alloy ($Cu_{73}Sn_{12}Si_{15}$)

In the isothermal section of the ternary Cu-Si-Sn system at 700 °C, a new ternary phase τ was found while analyzing BEI images and XRD patterns of the equilibrated samples in the Cu-rich region of 70-80 at.% Cu. Figure 2(a) shows the BEI image of alloy #7 containing 76 at.% Cu, 8 at.% Sn, and 16 at.% Si, in which η-$Cu_3Si$ phases exist in addition to the ternary τ compound, and there is another phase with a composition close to γ-bcc (D0_3). According to earlier reports on Cu-Sn alloys, γ-bcc (D0_3) should transform into δ-$Cu_{41}Sn_{11}$ or ε-$Cu_3Sn$ during quenching, and it is impossible to obtain a micrograph of γ-bcc (D0_3) at room temperature.[23] XRD analysis was therefore conducted to verify the phase constituents of sample #7. As shown in Fig. 3, the peaks denoted by filled square and unfilled circle symbols were a good match with the characteristic peaks of the η-$Cu_3Si$ phase and δ-$Cu_{41}Sn_{11}$, respectively, whereas the other peaks belong to be the ternary compound τ. So the phase in quenched sample #7 is η-$Cu_3Si$ phase, δ-$Cu_{41}Sn_{11}$, and τ. It must be pointed out that because δ-$Cu_{41}Sn_{11}$ or ε-$Cu_3Sn$ labeled in micrographs (Fig. 2) and XRD patterns (Fig. 3-5) was originally γ-bcc (D0_3) before quenching, phase label γ-bcc (D0_3) is kept in the ternary phase diagram of the Cu-Si-Sn system at 700 °C, and γ-bcc (D0_3) is also used to name the phase region. For the same reason as for sample #7, although the BEI image and XRD pattern of sample #11 sample containing 79 at.% Cu, 10 at.% Sn, and 11 at.% Si provided evidence of the

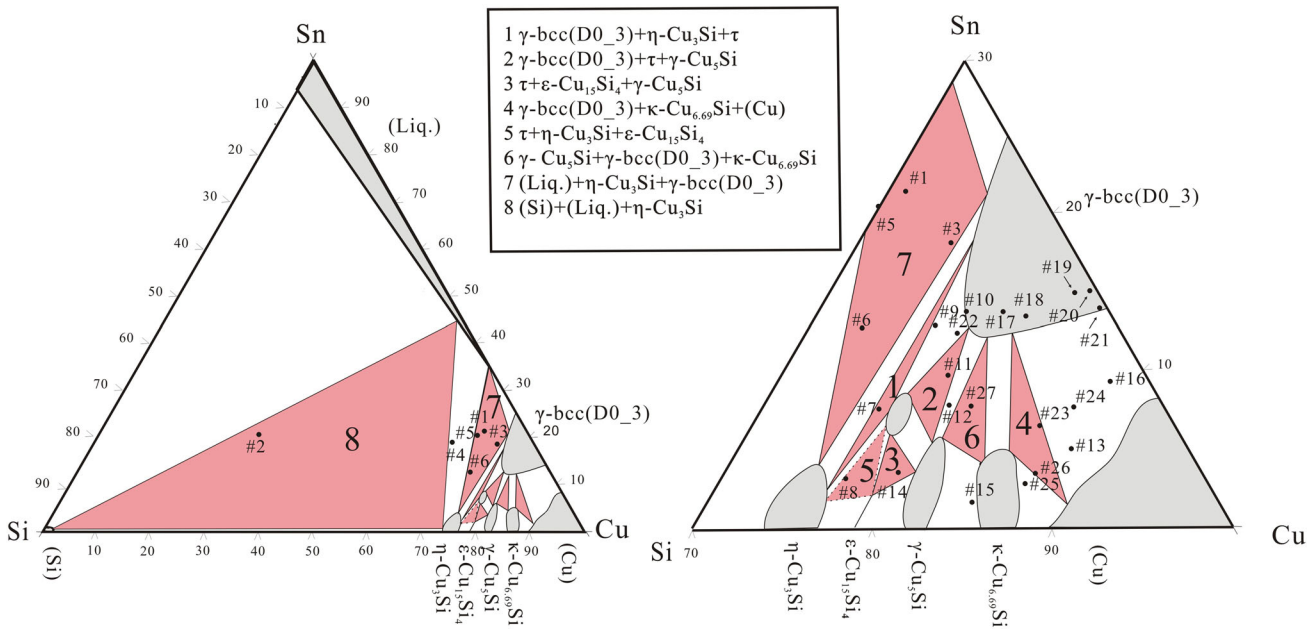


**Fig. 6** Phase relationships for the Cu-Si-Sn system, constructed from samples heat-treated at 700 °C

**Table 3 Summary of all the samples' nominal compositions and experimental results for Cu-Si-Sn alloys annealed at 500 °C**

| | Nominal composition | | | | Phase composition | | |
|---|---|---|---|---|---|---|---|
| No. | Cu | Sn | Si | Phase | Cu | Sn | Si |
| #31 | 30 | 30 | 40 | (Si) | 1.2 | 0.8 | 98 |
| | | | | Liq. | 8.5 | 89.9 | 1.6 |
| | | | | η′-$Cu_3Si$ | 72.9 | 2.6 | 24.5 |
| #32 | 73 | 14 | 13 | Liq. | 85.1 | 14.1 | 0.8 |
| | | | | η′-$Cu_3Si$ | 75.5 | 3.8 | 20.7 |
| | | | | ε-$Cu_3Sn$ | 75.5 | 23.9 | 0.6 |
| #33 | 77 | 6 | 17 | η′-$Cu_3Si$ | 74 | 4.5 | 21.5 |
| | | | | δ-$Cu_{41}Sn_{11}$ | 79.1 | 17.1 | 3.8 |
| | | | | ε-$Cu_3Sn$ | 75.4 | 23.2 | 1.4 |
| #34 | 79 | 7 | 14 | γ-$Cu_5Si$ | 82.2 | 1.1 | 16.7 |
| | | | | η′-$Cu_3Si$ | 76.5 | 4.8 | 18.7 |
| | | | | δ-$Cu_{41}Sn_{11}$ | 80 | 15.6 | 4.4 |
| #35 | 84 | 6 | 10 | (Cu) | 89.8 | 1.4 | 8.8 |
| | | | | γ-$Cu_5Si$ | 82.9 | 1.7 | 15.4 |
| | | | | δ-$Cu_{41}Sn_{11}$ | 81 | 16.7 | 2.3 |

existence of γ-$Cu_5Si$, δ-$Cu_{41}Sn_{11}$ and τ, sample #11 is actually located in the γ-$Cu_5Si$, γ-bcc (D0_3) and τ ternary-phase region. The equilibrated sample #14 containing 81 at.% Cu, 2 at.% Sn, and 17 at.% Si is a three-phase equilibrium of γ-$Cu_5Si$, ε-$Cu_{15}Si_4$, and τ (Fig. 2c). In addition, the τ phase was also identified in alloys #8, #9, and #22, as listed in Table 2. The XRD patterns of the three alloys, #7 ($Cu_{76}Sn_8Si_{16}$), #11 ($Cu_{79}Sn_{10}Si_{11}$), and #14 ($Cu_{81}Sn_2Si_{17}$), are presented together in Fig. 3, for comparison, where the presence of the τ phase is confirmed. According to EDS analysis on the samples containing the τ phase, the Cu and Sn content were 77-78.7, 5.8-9.8 at.%, respectively, and the surplus is Si content. The crystal structure of the new τ phase was analyzed by use of Jade 5.0 software. As shown in Fig. 3, characteristic peaks of the τ phase coincide well with that of δ-$Cu_{33}Si_7$, so the τ phase is inferred to have the same hexagonal structure as δ-$Cu_{33}Si_7$; the space group is $P6_3/mmc$, $a = 8.012$ nm, and $c = 5.04$ nm. The τ phase might be the δ-$Cu_{33}Si_7$ phase with added Sn. Because δ-$Cu_{33}Si_7$ exists in the temperature range 710-824 °C,[21] dissolution of Sn in δ-$Cu_{33}Si_7$ leads to stability of this phase at 700 °C, or even lower

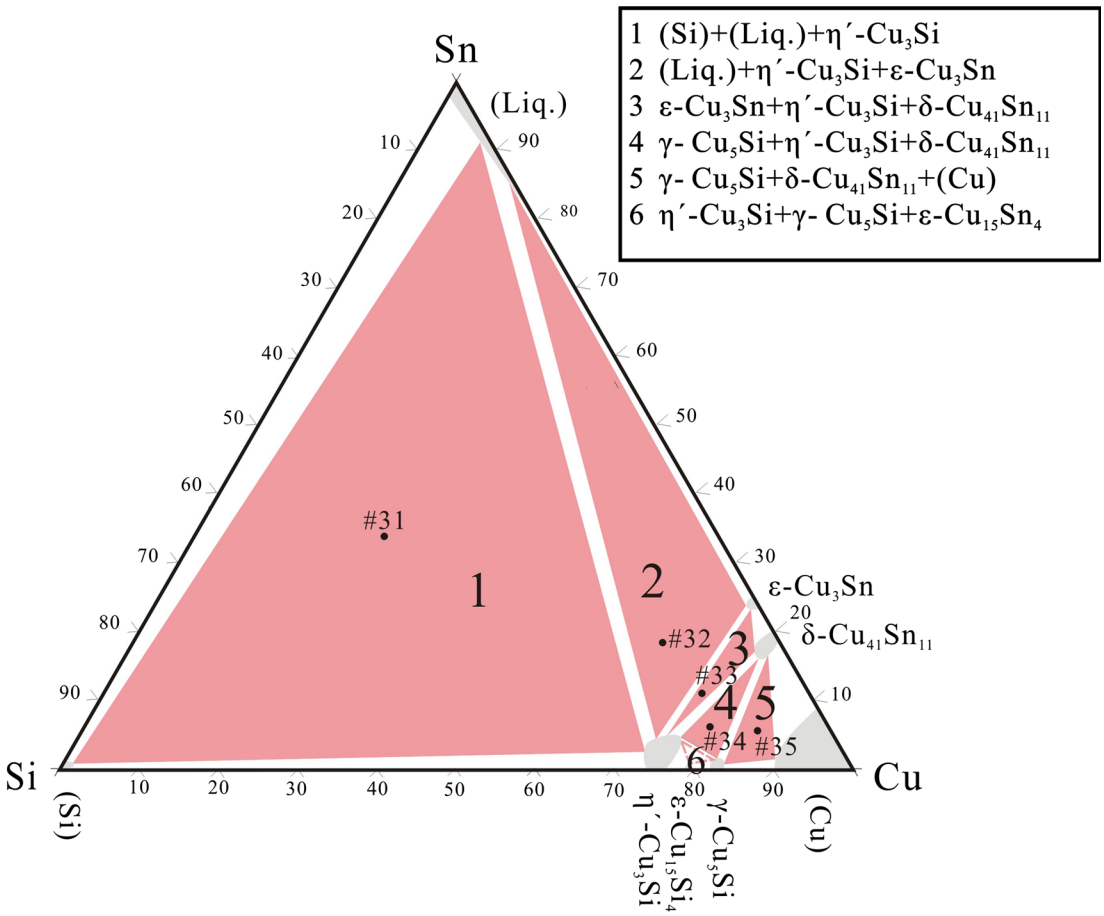


**Fig. 7** Phase relationships for the Cu-Si-Sn system at 500 °C

temperature. However, more experiments are needed to verify this inference.

The BEI image and XRD pattern of alloy #23 ($Cu_{86}Sn_7Si_7$) are shown in Fig. 2d and 4, respectively. In Fig. 2d, the dark gray areas correspond to the (Cu) phase, the light gray areas are the κ-$Cu_{6.69}Si$ phase with the composition 85.4 at.% Cu-8.3 at.% Sn-6.3 at.% Si, and the composition of the white areas is close to that of the transformed γ-bcc (D0_3) phase. Its XRD pattern is presented in Fig. 4, where the characteristic peaks of the (Cu) and κ-$Cu_{6.69}Si$ phases are well marked by unfilled square and unfilled circle symbols, respectively, and all the other peaks correspond to the δ-$Cu_{41}Sn_{11}$ phase. Because the δ-$Cu_{41}Sn_{11}$ phase at room temperature originated from the γ-bcc (D0_3) phase by a peritectoid reaction (γ-bcc (D0_3) + ζ-$Cu_{10}Sn_3$ → δ-$Cu_{41}Sn_{11}$), sample #23 located in the three-phase region of (Cu), κ-$Cu_{6.69}Si$ and γ-bcc (D0_3).

Because τ is in equilibrium with η-$Cu_3Si$ or ε-$Cu_{15}Si_4$, as observed for alloys #7 and #14, respectively, on the basis of the phase rule it is believed that a ternary-phase region of τ + η-$Cu_3Si$ + ε-$Cu_{15}Si_4$ at 700 °C should exist. A three phase equilibrium between γ-$Cu_5Si$, γ-bcc (D0_3), and κ-$Cu_{6.69}Si$ has been observed for alloy #27 in the Cu-rich corner of 80-90 at.% Cu.

Figure 2d shows the BEI image of alloy #6, three regions with different contrast are illustrated: the dark gray, light grey, and white part region. The dark gray region part contains 75 at.% Cu and 24.5 at.% Si with small Sn solubility. It corresponds to the η-$Cu_3Si$ phase, on the basis of the binary phase diagram. The light grey part contains 76.3 at.% Cu, 21.9 at.% Sn, and a limited amount of Si, with a composition close to that of γ-bcc (D0_3). The white region with the black particles, with a mean area composition of 56.8 at.% Cu, 43 at.% Sn, and 0.2 at.% Si, corresponds to the liquid phase at 700 °C. However, it is difficult to identify the phase composition of the very small black particles. XRD analysis of this alloy was conducted, and its XRD pattern is illustrated in Fig. 5. In addition to the typical peaks for η-$Cu_3Si$ and Sn, additional peaks of ε-$Cu_3Sn$ and η-$Cu_6Sn_5$ are obvious. According to the Cu-Sn phase diagram, the solubility of Cu in the liquid phase is 33.1 at.% at 700 °C, and ε-$Cu_3Sn$ could be formed by decomposition of γ-bcc (D0_3) during solidification if the cooling rate is not quite fast enough; the η-$Cu_6Sn_5$ might be formed by the peritectic reaction ε-$Cu_3Sn$ + Liq. → η-$Cu_6Sn_5$. Therefore, the average chemical composition of the Liq. and η-$Cu_6Sn_5$ in the white region was regarded as the liquid composition. This ternary phase region (γ-bcc

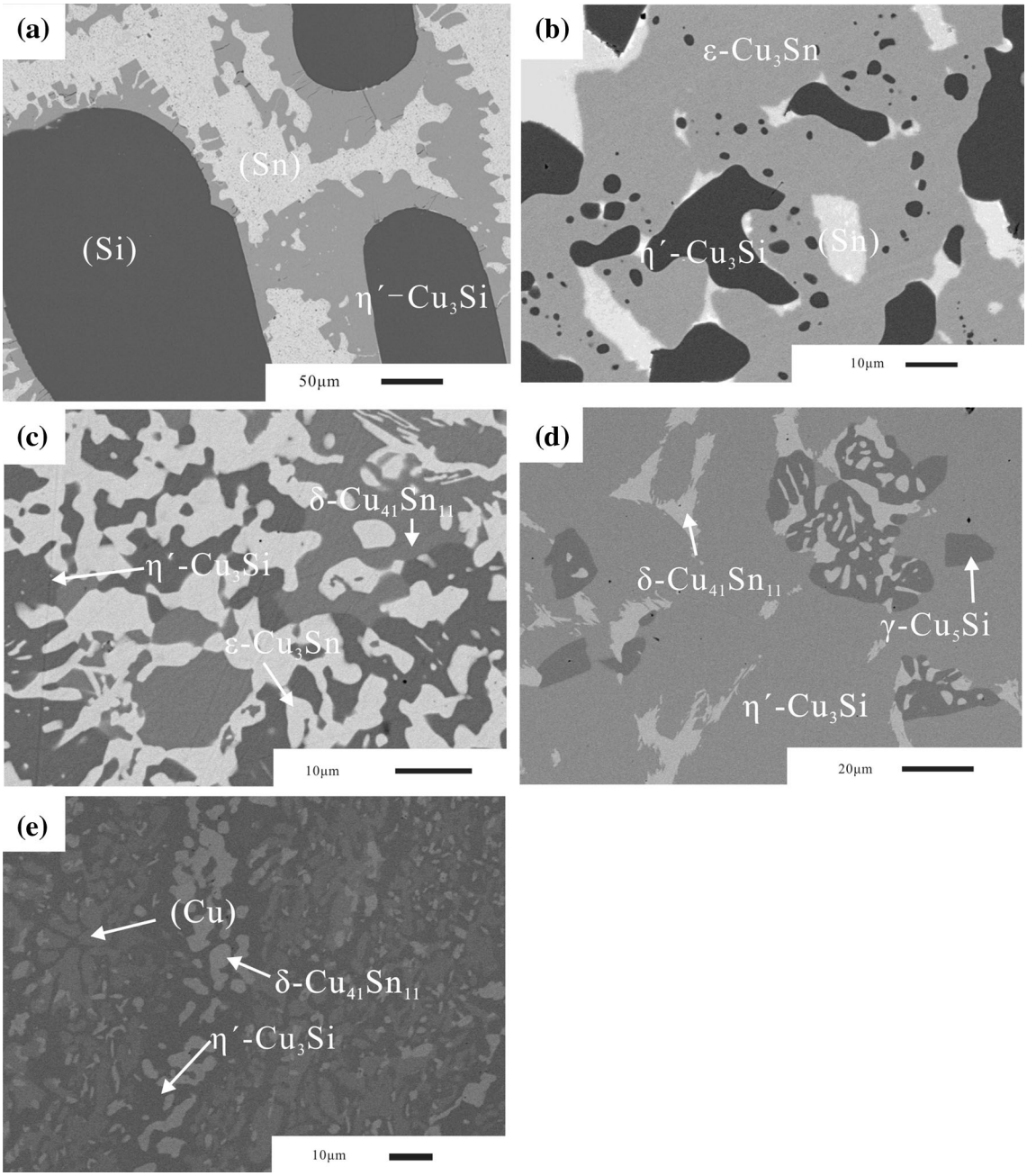


**Fig. 8** Images of the microstructure of typical ternary Cu-Si-Sn alloys annealed at 500 °C for 30 days. (a) sample #31 ($Cu_{30}Sn_{30}Si_{40}$), (b) sample #32 ($Cu_{73}Sn_{14}Si_{13}$), (c) sample #33 ($Cu_{76}Sn_6Si_{17}$), (d) sample #34 ($Cu_{79}Sn_7Si_{14}$), (e) sample #35 ($Cu_{84}Sn_6Si_{10}$)

(D0_3) + η-$Cu_3Si$ + Liq.) was also evident for alloys #1, #3, and #5.

The Cu-poor part of the triangle is a unique ternary-phase region consisting of the Si, Liq., and η-$Cu_3Si$ phases according to SEM-EDS analysis of alloy#2 ($Cu_{30}Sn_{20}Si_{50}$).

On the basis of the results obtained in this work an isothermal section of the Cu-Si-Sn system at 700 °C was constructed, as shown in Fig. 6. This isothermal section consists of eight ternary-phase regions:

1. η-$Cu_3Si$ + γ-bcc (D0_3) + τ,
2. γ-bcc (D0_3) + γ-$Cu_5Si$ + τ,
3. γ-$Cu_5Si$ + τ + ε-$Cu_{15}Si_4$,
4. γ-bcc (D0_3) + (Cu) + κ-$Cu_{6.69}Si$,
5. τ + η-$Cu_3Si$ + ε-$Cu_{15}Si_4$,
6. γ-$Cu_5Si$ + γ-bcc (D0_3) + κ-$Cu_{6.69}Si$,
7. η-$Cu_3Si$ + γ-bcc (D0_3) + Liq., and
8. η-$Cu_3Si$ + Liq. + (Si).

The deduced ternary-phase region is illustrated with a dotted line in Fig. 6. Most of the equilibria are located at the Cu-rich corner, and the γ-bcc (D0_3) phase equilibrates at 700 °C with all the binary phases except ε-$Cu_{15}Si_4$.

### 3.2 Phase Equilibria of the Cu-Si-Sn System at 500 °C

The isothermal section of the Cu-Si-Sn system at 500 °C was studied in the whole concentration range with special attention to the region in the vicinity of the new ternary phase τ, which was first found at 700 °C. In this region, most of the changes observed at 700 °C were evidenced. On the basis of the compositions determined in the two-phase and three-phase regions summarized in Table 3, the phase equilibria of the Cu-Si-Sn system at 500 °C are shown graphically in Fig. 7.

The unary and binary phases in the Cu-Si and Cu-Sn binary systems at 500 °C were confirmed except for the ε-$Cu_{15}Si_4$ phase. Although the ε-$Cu_{15}Si_4$ phase should be stable at 500 °C according the binary phase diagram of the Cu-Si system,[3,4] only η′-$Cu_3Si$ and γ-$Cu_5Si$ were observed experimentally and only small variations of the homogeneity ranges of η′-$Cu_3Si$ and γ-$Cu_5Si$ occurred. For the Cu-Sn binary system, the ε-$Cu_3Sn$ and δ-$Cu_{41}Sn_{11}$ phases were present and a small solid solution limited to less than 1.4 at.% Si in ε-$Cu_3Sn$ was formed. Because the newly determined phase τ was not observed at 500 °C, the phase relationships in the Cu-rich region have obviously changed.

The microstructures of alloys #30-35 observed by SEM are shown in Fig. 8a-e, respectively. Because phases in an alloy can be easily differentiated on the basis of on the relief, color, and chemical composition, ternary phase regions of:

1. (Si) + Liq. + η′-$Cu_3Si$,
2. Liq. + η′-$Cu_3Si$ + ε-$Cu_3Sn$,
3. η′-$Cu_3Si$ + δ-$Cu_{41}Sn_{11}$ + ε-$Cu_3Sn$,
4. γ-$Cu_5Si$ + η′-$Cu_3Si$ + δ-$Cu_{41}Sn_{11}$, and
5. (Cu) + γ-$Cu_5Si$ + δ-$Cu_{41}Sn_{11}$

can be easily identified by referring to Fig. 8a-e, respectively. Except for the above three-phase regions, coexistence of η′-$Cu_3Si$, ε-$Cu_{15}Si_4$ and γ-$Cu_5Si$ was not observed in this work. However, it can be deduced on the basis of the phase relationships in the vicinity according to the phase rule. This ternary region has been included, denoted with the dotted line in Fig. 7.

## 4. Summary

SEM-EDS analysis and XRD studies were used to construct phase relationships for the Cu-Si-Sn ternary system at 700 and 500 °C on the basis of equilibrated alloys. The isothermal section at 700 °C consists of nine single-phase regions, sixteen two-phase regions, and eight three-phase regions.

A previously unknown ternary phase τ with a possible homogeneity interval in the range $Cu_{76}Sn_{7.8}Si_{16.2}$-$Cu_{85}Sn_{7.6}Si_{7.4}$ was found at 700 °C for the first time. The τ phase has the same hexagonal structure as δ-$Cu_{33}Si_7$; the space group is $P6_3/mmc$ with $a$ = 8.012 nm and $c$ = 5.04 nm. The maximum solid solubility of Sn in η′-$Cu_3Si$ is 5.6 at.%, and that of Si in γ-bcc (D0_3) is 12.8 at.%. Dissolution of Sn in δ-$Cu_{33}Si_7$ leads to this phase becoming stable at 700 °C, or at an even lower temperature. However, more experiments are needed to verify this inference.

Eight single-phase regions, thirteen two-phase regions, and six three-phase regions were observed in the isothermal region of the Cu-Si-Sn system at 500 °C. The solubilities of Sn in η′-$Cu_3Si$ and γ-$Cu_5Si$, and those of Si in ε-$Cu_3Sn$ and δ-$Cu_{41}Sn_{11}$ were 4.8, 1.7, 1.4, and 4.4 at.%, respectively. Study of the isothermal region at 500 °C revealed no evidence of the newly identified ternary phase τ.


## Acknowledgments

Financial support from the National Science Foundation of China (grant nos 51171031 and 51271041) and a Project Funded by the Priority Academic Program Development of Jiangsu Higher Education Institutions is gratefully acknowledged.


## References


1. B.P. Richards, C.L. Levoguer, C.P. Hunt, K. Nimmo, S. Peters, and P. Cusack, An Analysis of the Current Status of Lead-Free Soldering, NPL, ITRI and DTI Joint Report About Pb-free Soldering, January 1999
2. IPC Roadmap, *Guide for Assembly of Lead-Free Electronics*, IPC, Northbrook, IL, 2000
3. M. Abtew and G. Selvaduray, Lead-Free Solders in Microelectronics, *Mater. Sci. Eng. R*, 2000, **27**(5), p 95-141
4. K. Suganuma, Advances in Lead-Free Electronics Soldering, *Curr. Opin. Solid State Mater. Sci.*, 2001, **5**(1), p 55-64
5. K.N. Tu and R.D. Thompson, Kinetics of Interfacial Reaction in Bimetallic Cu-Sn Thin Films, *Acta Metall.*, 1982, **30**(5), p 947-952
6. A.J. Sunwoo, J.W. Morris, and G.K. Lucey, The Growth of Cu-Sn Intermetallics at a Pretinned Copper-Solder Interface, *Metall. Trans. A*, 1992, **23**(4), p 1323-1332
7. B.J. Lee, N.M. Hwang, and H.M. Lee, Prediction of Interface Reaction Products Between Cu and Various Solder Alloys by Thermodynamic Calculation, *Acta Mater.*, 1997, **45**(5), p 1867-1874
8. S. Bader, W. Gust, and H. Hieber, Rapid Formation of Intermetallic Compounds Interdiffusion in the CuSn and NiSn Systems, *Acta Metall.*, 1995, **43**(1), p 329-337
9. D.R. Frear, D. Grivas, and J.W. Morris, Parameters Affecting Thermal Fatigue Behavior of 60Sn-40Pb Solder Joints, *J. Electron. Mater.*, 1989, **18**, p 671-680
10. P.L. Tu, Y.C. Chan, and J.K.L. Lai, Effect of Intermetallic Compounds on the Thermal Fatigue of Surface Mount Solder Joints, *IEEE Trans. Compon. Packag. Manuf. Technol. B*, 1997, **20**(1), p 87-93
11. Y.C. Chan, P.L. Tu, A.C. So, and J.K.L. Lai, Effect of Intermetallic Compounds on the Shear Fatigue of Cu/63Sn-

37Pb Solder Joints, IEEE Trans, *Compon. Packag. Manuf. Technol. B*, 1997, **20**(4), p 463-469
12. L. Quan, D. Frear, D. Grivas, and J.W. Morris, Tensile Behavior of Pb-Sn Solder/Cu Joints, *J. Electron. Mater.*, 1987, **16**(3), p 203-208
13. R.E. Pratt, E.I. Stromswold, and D.J. Quesnel, Effect of Solid-State Intermetallic Growth on the Fracture Toughness of Cu/63Sn-37Pb Solder Joints, *Compon. Packag. Manuf. Technol. A*, 1996, **19**(1), p 134-141
14. M.H. Lee, D.H. Bae, D.H. Kim, and D.J. Sordelet, Synthesis of Ni-Based Bulk Metallic Glass Matrix Composites Containing Ductile Brass Phase by Warm Extrusion of Gas Atomized Powders, *J. Mater. Res.*, 2003, **18**(09), p 2101-2108
15. N.F. Lashko, K.P. Sorokina, and A.N. Gorbunov, Strengthening of Silicon Monel, *Met. Sci. Heat Treat.*, 1996, **6**, p 48-49
16. H. Okamoto, Cu-Si (Copper-Silicon), *J. Phase Equilib. Diffus.*, 2012, **33**(5), p 415-416
17. D. Shin, J.E. Saal, and Z.K. Liu, Thermodynamic Modeling of the Cu-Si System, *CALPHAD*, 2008, **32**(3), p 520-526
18. J.H. Shim, C.S. Oh, B.J. Lee, and D.N. Lee, Thermodynamic Assessment of the Cu-Sn System, *Z. Metallk.*, 1996, **87**(3), p 205-212
19. J. Miettinen, Thermodynamic Description of the Cu-Al-Sn System in the Copper-Rich Corner, *Metall. Mater. Trans. A*, 2002, **33**(6), p 1639-1648
20. X.J. Liu, C.P. Wang, I. Ohnuma, R. Kainuma, and K. Ishida, Experimental Investigation and Thermodynamic Calculation of the Phase Equilibria in the Cu-Sn and Cu-Sn-Mn Systems, *Metall. Mater. Trans. A*, 2004, **35**, p 1641-1654
21. W. Gierlotka, S.W. Chen, and S.K. Lin, Thermodynamic Description of the Cu-Sn System, *J. Mater. Res.*, 2007, **22**(11), p 3158-3165
22. M. Li, Z.M. Du, C.P. Guo, and C.R. Li, Thermodynamic Optimization of the Cu-Sn and Cu-Nb-Sn Systems, *J. Alloys Compd.*, 2009, **477**(1), p 104-117
23. S. Fürtauer, D. Li, D. Cupid, and H. Flandorfer, The Cu-Sn Phase Diagram, Part I: New Experimental Results, *Intermetallics*, 2013, **34**, p 142-147
24. D. Li, P. Franke, S. Fürtauer, D. Cupid, and H. Flandorfer, The Cu-Sn Phase Diagram Part II: New Thermodynamic Assessment, *Intermetallics*, 2013, **34**, p 148-158
25. H.L. Lukas, I. Ansara, A.T. Dinsdale, and M.H. Rand (Eds.), *COST507—Thermochemical Database for Light Metal Alloys*, Vol. 18499, 1998, p 224-226
26. V.T. Deshpande and D.B. Direshmukh, Thermal Expansion of Tin in the β-γ Transition Region, *Acta Crystallogr.*, 1962, **15**, p 294-295
27. M. Kantola and E. Tokola, X-ray Studies on the Thermal Expansion of Copper-Nickel Alloys, *Ann. Acad. Sci. Fenn.*, 1967, **223**, p 1-10
28. J.A. Lee and G.V. Raynor, The Lattice Spacings of Binary Tin-Rich Alloys, *Proc. Phys. Soc. B*, 1954, **67**(10), p 737
29. H. Knödler, Über Kristallstruktur und strukturellen Zusammenhang der Phasen gamma und epsilon im System Kupfer-Zinn, *Metall*, 1966, **20**(8), p 823-829, in German
30. M.H. Booth, J.K. Brandon, R.Y. Brizard, C.T. Chieh, and W.B. Pearson, Brasses with F Cells, *Acta Crystallogr. Sect. B Struct. Sci.*, 1977, **33**(1), p 30-36
31. J.K. Brandon, W.B. Pearson, and D.J.N. Tozer, A Single-Crystal X-ray Diffraction Study of the ζ Bronze Structure, Cu20Sn6, *Acta Crystallogr. Sect. B Struct. Sci.*, 1975, **31**(3), p 774-779
32. Y. Watanabe, Y. Fujinaga, and H. Iwasaki, Lattice Modulation in the Long-Period Superstructure of $Cu_3Sn$, *Acta Crystallogr. Sect. B Struct. Sci.*, 1983, **39**(3), p 306-311
33. A. Gangulee, G.C. Das, and M.B. Bever, An X-ray Diffraction and Calorimetric Investigation of the Compound $Cu_6Sn_5$, *Metall. Trans. A*, 1973, **4**(9), p 2063-2066
34. A.K. Larsson, L. Stenberg, and S. Lidin, The Super-Structure of Domain-Twinned eta′-$Cu_6Sn_5$, *Acta Crystallogr. Sect. B Struct. Sci.*, 1994, **50**, p 636-643
35. PDF #51-0915, JCPDS-ICDD P. Version 2.2, 2001. Original from: L. Chen, List of Precious Metals, Kunming, P.R. China, Private Communication, 1998
36. S. Arrhenius and A. Westgren, X-radiation Analysis of Copper-Silicon Alloys, *Z. Phys. Chem.*, 1931, **14**, p 66-79
37. F.R. Morral and A. Westgren, Ark, *Kemi Mineral. Geol. B*, 1934, **11**, p 1-6
38. K.P. Mukherjee, J. Bandyopadhyay, and K.P. Gupta, Phase Relationship and Crystal Structure of Intermediate Phases in the Cu-Si System in the Composition Range of 17 to 25 at.% Si, *Trans. Metall. Soc. AIME*, 1969, **245**, p 2335-2338